

## Beam current-density dependence of the polarization of emission lines from foil-excited atoms: Beam dose dependent or field dependent

Yasuyuki Kimura and Keishi Ishii

*Department of Engineering Physics and Mechanics, Faculty of Engineering, Kyoto University, Kyoto 606-01, Japan*

(Received 28 October 1997)

We have observed linearly polarized components of the foil-excited hydrogen Balmer  $\alpha$  line and the neutral helium  $2^1P-3^1D$  line from beams of  $5-55 \mu\text{A}/\text{cm}^2$  current density at 150 keV. The intensities and the linear Stokes parameter of both the lines changed with the total beam charge density irradiated to the carbon foil (beam dose) and then saturated. These changes are attributed to changes of the state of the carbon foil caused by the irradiation by the ion beam. The dose dependence of the linear Stokes parameter was fitted with an exponential curve. The values at saturation for both the lines showed an increase with an increase in the current density, which is similar to the previous reports. The initial value for the helium line depended little on the beam current density, while that for the hydrogen line showed substantial increase. Both the behaviors are consistent with the explanation in terms of the Stark effect by the macroscopic electric field of the order of 10 V/cm extending downstream from the foil. [S1050-2947(98)03205-3]

PACS number(s): 34.50.Fa, 32.60.+i, 33.20.Kf

### I. INTRODUCTION

In beam foil spectroscopy, light emitted from atoms or ions excited on passage through a thin carbon foil is observed downstream of the foil. When the foil is oriented normal to the beam direction, linear polarization (expressed with the linear Stokes parameter  $M/I$ ) is observed. The foil may be tilted, then circular polarization appears and the polarization characteristics are expressed in terms of the Stokes parameters. All the polarization characteristics depend on the states of the excited atoms created by the interaction between the ion or the atom and the foil.

Berry *et al.* [1] observed the neutral helium  $2^1S-3^1P$  line and found changes in the Stokes parameters against the tilt angle. Eck [2] proposed a model: when an atom was located in the vicinity of the foil within a few Bohr radii, it was perturbed by an image dipole electric field (“microscopic” surface field), which was directed normal to the foil with the strength of the order of  $10^8$  V/cm and fell off rapidly with distance from the foil. As its results, alignment, orientation, and coherence were produced in the ensemble of the excited atoms. Subsequently, many experiments [3–5] were reported for neutral helium transitions, along with calculations [6,7]. For example, by fitting the calculation to the Brooks *et al.* [5] experiment, Weber *et al.* [8] obtained a field of  $6.2 \times 10^5$  V/cm extending from the foil surface over a distance of 8.64 nm downstream.

Hight *et al.* [9] found that, for the normal incident beam, the linear Stokes parameter  $M/I$  of the neutral helium  $2^1S-3^1P$  line increased with an increase in the ion beam current density. Winter [10] did a similar experiment on the helium  $2^1P-3^1D$  line and applied the microscopic surface field shielded by secondary electrons. The field strength was estimated to be  $\sim 10^8$  V/cm. Gay *et al.* [11,12] tried to explain the current density dependence as due to the change in the foil temperature by the beam irradiation through the change in the secondary electron cloud density.

Singer *et al.* [13] found that  $M/I$  of the hydrogen Balmer  $\beta$  line also increased with an increase in the ion beam current density. They explained the increase by assuming a “macroscopic” field that was due to the potential distribution at the foil surface. Its strength was proportional to the beam current density with the order of  $1 \sim 10$  V/cm. Dehaes *et al.* [14] developed the macroscopic field model further. They measured the total intensity and linear polarization of the Balmer series lines ( $n=2-n'$ ,  $4 \leq n' \leq 9$ ) as a function of the beam current. They explained the result by assuming the macroscopic electric field produced by a uniform charge distribution or a uniform potential on the foil surface. They confirmed that the electric field increased with the beam current and that it acted over a distance of a few millimeters downstream from the foil.

The above arguments show that we have not reached a point where we have a coherent explanation of the polarization of emission lines and its current density dependence. For example, the field strength proposed by various authors ranges from  $10^{0-1}$  V/cm to  $10^8$  V/cm. This large divergence stems partly from the following fact: The energy differences between levels,  $E_{nL} - E_{nL'}$  ( $L \neq L'$ ) of helium atoms are about 3 orders larger than those of hydrogen atoms. Hence, the field required for the Stark mixing of the levels is 3 orders higher for helium than for hydrogen. On the other hand, the microscopic surface field strength is independent of the irradiated ion species. The macroscopic field may be due to the charge accumulating on the foil surface resulting from neutralization of the ions and secondary electron emission by the foil. Since the yield of the secondary electron emission [15] and the neutralization ratio should be similar for proton and helium ion passages, the strength of the macroscopic field should be similar for both the atomic species.

Recently, Harper *et al.* [16] measured the tilt angle dependence of the Stokes parameters of the hydrogen Balmer  $\alpha$  line. They found that the polarization characteristics depended on the irradiated beam charge density to the foil (it is

called “*beam dose*”). They suggested that the beam dose dependence was brought about by the graphitization of the foil induced by the beam irradiation. If this explanation is correct, we have to take into account the dose effect in the beam current density dependence of the polarization characteristics.

In order to understand the polarization characteristics of the foil excited atoms, we have first to separate the beam dose effect. In the following experiment we follow the beam dose of the foil from the very beginning of beam irradiation. We then discuss the current density dependence.

## II. EXPERIMENTAL SETUP

A beam of protons ( $H^+$ ) or helium ions ( $He^+$ ) was produced by an electrostatic accelerator, and it was led through the beam line to the collision chamber. On the beam line, a movable Faraday cup (beam line Faraday cup) was placed, which was used to interrupt the beam and to measure the beam current. The pressure inside the chamber was about  $5 \times 10^{-7}$  torr. A target foil and the observation region along the beam were surrounded by a grounded inner cell (150 mm  $\times$  40 mm  $\times$  120 mm) made of Permalloy plate (0.3 mm thick), which had an entrance hole (3.0 mm diameter) and an exit hole (16.0 mm diameter). The entrance hole acted as an aperture to limit the beam diameter hitting the target foil. The inner cell had also a slit (15 mm  $\times$  100 mm) for handling the target foil and an opening (115 mm  $\times$  10 mm) for observation of light emanating from the beam. The inside surface of the inner cell was painted black so as to reduce the light reflection by it. The purpose of adopting the cell was to shield magnetic and electric fields outside. The Earth’s magnetic field inside was estimated to be less than 0.01 G. Therefore, the motional electric field was less than 0.04 V/cm for hydrogen atoms traveling with an energy of 150 keV and was well neglected.

The foil was self-supported on a grounded aluminum holder having an opening diameter of 4.0 mm. It was placed 25.0 mm downstream from the aperture of 3.0 mm diameter. For the proton beam, foils of surface density  $3 \mu\text{g}/\text{cm}^2$  (MICROMATTER CO.) were used. For the helium ion beam, those of  $5 \mu\text{g}/\text{cm}^2$  (Atomic Energy of Canada Limited Research Development Company) were used. Seven foil holders were set on a disk that was rotated from outside. One of the foil holders was set inside the inner cell, so that the beam passed through the center circular area of 3 mm diameter of the foil.

After the passage of the beam through the carbon foil, a part (less than 5% for a 150-keV  $H^+$  beam and  $3 - \mu\text{g}/\text{cm}^2$  foil) of the ions was neutralized and the rest remained as ions. This beam was collected by another Faraday cup (chamber side Faraday cup) far downstream of the foil. The beam current was integrated, digitized (ORTEC 439) with  $10^2$  pulse/ $\mu\text{C}$  or  $10^4$  pulse/ $\mu\text{C}$ , counted, and finally transferred to a personal computer. A ring electrode having an aperture of 16.0 mm diameter, and biased to  $-200$  V to the ground potential was placed just in front of the Faraday cup. This electrode prevented the secondary electrons from coming into the Faraday cup and also prevented secondary electrons produced inside the cup from going out. Owing to the inner cell, this electric potential did not affect the atoms up-

stream in the observation region.

Through the opening of the inner cell and the fused quartz window (35 mm diameter, 5 mm thickness) on the side wall of the chamber, we observed the light emitted from the beam. The optical axis was directed perpendicularly to the beam direction. The light from the beam made parallel by the first lens (50 mm diameter, 280 mm focal length) went through a polarizer and an interference filter for wavelength selection and was focused by the second lens (same as the first one) on a slit in front of a photomultiplier tube (PMT) with one-to-one imaging.

The polarizer (for photographic camera, diameter 55 mm) was rotated around the optical axis with  $90^\circ$  steps by a stepping motor that was controlled by the personal computer. The interference filter for the hydrogen Balmer  $\alpha$  transition (656.3 nm) had a 656.9-nm center wavelength, 81% maximum transmission, 17-nm full width at half maximum (FWHM), and 30-mm diameter. That for the helium  $2^1P-3^1D$  transition (667.8 nm), had a 669-nm center wavelength, 71% maximum transmission, 12-nm FWHM, and 30-mm diameter.

The observation region of the beam was determined by the slit in front of the PMT. The width was 7.0 mm and thus the observation region was the part of the beam from 12.5 mm to 19.5 mm downstream of the foil. The PMT (EMI 9863B) was cooled by a Peltier element to reduce thermal noise. The output photoelectron pulses were counted by the conventional photon counting system, and transferred to the personal computer.

## III. RESULTS

One measurement started when we began irradiating the virgin foil with the proton beam. At the same time we began our measurement steps. One step consisted of four substeps: (i) with the transmission axis of the polarizer parallel to the beam direction, the number of photoelectron pulses was counted for 5 s (photon counts), and the beam current was measured by the chamber side Faraday cup. If the beam current deviated by more than  $\pm 10\%$  from a preset value, the ion beam current was adjusted and then the procedure was repeated. For another 5 s, the number of photoelectron pulses was counted. The polarizer was rotated by  $90^\circ$ . (ii) The number of pulses was counted and the beam current was measured simultaneously for  $2 \times 5$  s, and the polarizer was rotated further by  $90^\circ$ . (iii), (iv) Similar procedures were followed. We define the intensity of the parallel component  $I^{\parallel}$  as the sum of the photon counts of the substeps (i) and (iii) divided by the ion charge collected during these substeps. The perpendicular component intensity  $I^{\perp}$  is similarly defined.

An example of the results for the hydrogen Balmer  $\alpha$  line is shown in Fig. 1:  $I^{\parallel}$  and  $I^{\perp}$  are shown. The beam energy is 150 keV, and the ion beam current density is  $48 \mu\text{A}/\text{cm}^2$ . The statistical uncertainty represented by PE (typical value is  $\sim 0.03$  in the same units of intensity) is smaller than the magnitude of the symbol. The abscissa represents the total dose from the beginning of the irradiation in the units of  $\text{mC}/\text{cm}^2$ . It was determined from the current at the chamber side Faraday cup, so that the actual dose is estimated to be higher by  $\sim 5\%$ .

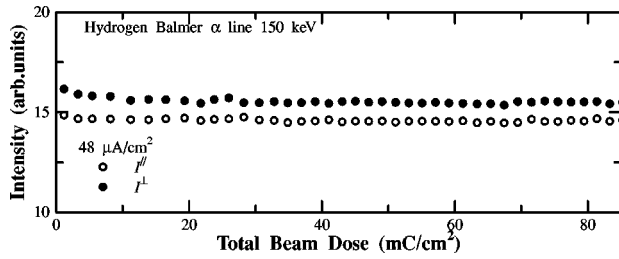


FIG. 1. The observed intensities of the polarized components  $I^{\parallel}$  (open circles) and  $I^{\perp}$  (filled circles) of the hydrogen Balmer  $\alpha$  line in the course of beam irradiation. The abscissa represents the total beam dose from the beginning of the irradiation in units of  $\text{mC}/\text{cm}^2$ . The beam energy is 150 keV, and the ion beam current density is  $48 \mu\text{A}/\text{cm}^2$ .

Figure 1 shows that both intensities  $I^{\parallel}$  and  $I^{\perp}$  decrease during the initial stage of irradiation and saturate. This initial transient is faster with the parallel component  $I^{\parallel}$  than with the perpendicular one  $I^{\perp}$ . This feature is common to other beam current densities.

The linear Stokes parameter  $M/I = (I^{\parallel} - I^{\perp}) / (I^{\parallel} + I^{\perp})$  is shown in Fig. 2 with the open circles. The bar represents the statistical uncertainty. As is expected from Fig. 1, the linear Stokes parameter  $M/I$  shows an initial increase and saturates. It is noted that in this report, when  $M/I$  is negative, ‘‘an increase of  $M/I$ ’’ corresponds to a decrease of its absolute value. We fit this dose dependence with

$$[M/I](Q) = [M/I]_S [1 - \exp(-Q/\tau)] + [M/I]_0 \exp(-Q/\tau), \quad (1)$$

where  $Q$  is the total dose, and the  $\tau$  is the ‘‘dose’’ constant. ‘‘0’’ and ‘‘S’’ denote, respectively, the initial and the saturated value. The result of  $[M/I]_0$  and  $[M/I]_S$  is given in Fig. 3. Figure 2 also shows the dose dependence of  $M/I$  for a lower current density,  $6 \mu\text{A}/\text{cm}^2$ , with the open squares. One point represents the average over 4 steps. A similar

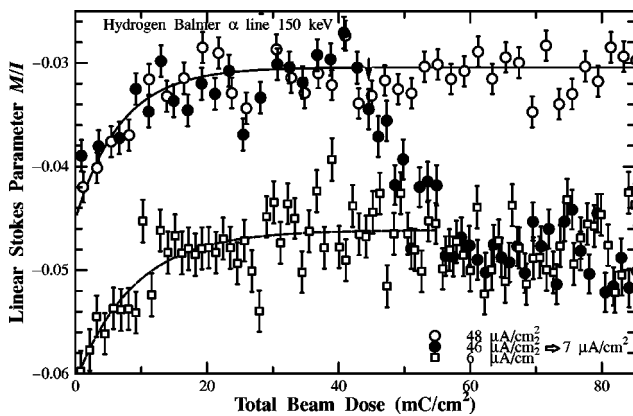


FIG. 2. The linear Stokes parameter  $M/I$  of the hydrogen Balmer  $\alpha$  line against the beam dose. The abscissa is the same as Fig. 1. The open circles are for the current density of  $48 \mu\text{A}/\text{cm}^2$ , and the open squares are for  $6 \mu\text{A}/\text{cm}^2$ . The filled circles represent the  $M/I$  when the beam current density was started with  $46 \mu\text{A}/\text{cm}^2$  and at  $44 \text{mC}/\text{cm}^2$  it was changed to  $7 \mu\text{A}/\text{cm}^2$ . The vertical arrow represents the first datum with the lower density  $7 \mu\text{A}/\text{cm}^2$ . The two curves represent the fitting by Eq. (1).

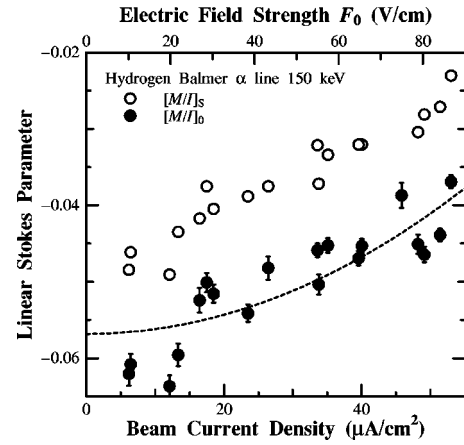


FIG. 3. The beam current density dependence of the initial value  $[M/I]_0$  (filled circles) and the saturated value  $[M/I]_S$  (open circles). The broken curve represents the fitted  $M/I$  calculated with the macroscopic field model, and the top abscissa is the field strength thus determined.

feature to the higher density case is seen. The initial  $[M/I]_0$  and the saturated  $[M/I]_S$  from the fitting (dotted curve) are also given in Fig. 3. As is suggested by the goodness of the fit (the reduced chi square is 1.2 and 0.8, respectively, for these two cases), the dose dependence is well expressed by Eq. (1). Figure 3 includes results for other current densities. For all  $[M/I]_0$  and  $[M/I]_S$ , the reduced chi squares of the fitting are within the range 0.8–1.5.

We may draw two conclusions here: (i) The linear Stokes parameter  $M/I$  increases with an increase in the dose and saturates with the ‘‘dose’’ constant  $\tau$  of  $4 \sim 14 \text{mC}/\text{cm}^2$ . (ii) Both  $[M/I]_0$  and  $[M/I]_S$  increase with an increase in the beam current density.

Figure 2 includes an example represented with the closed circles in which the beam current density was started with  $46 \mu\text{A}/\text{cm}^2$  and at  $44 \text{mC}/\text{cm}^2$  it was changed to  $7 \mu\text{A}/\text{cm}^2$ . For the latter current density, one point represents the average over 4 steps. The vertical arrow represents the first (averaged) datum with the lower density  $7 \mu\text{A}/\text{cm}^2$ . For the beam reduction procedure, it took about 4 minutes of beam interruption, which corresponds  $\sim 6$  steps for the  $46 \mu\text{A}/\text{cm}^2$  data or  $\sim 1.5$  averaged steps for  $7 \mu\text{A}/\text{cm}^2$ . We found no appreciable difference in the behaviors for different interruption periods.

We may draw another two conclusions: (iii) The saturated value is independent of the dose history of the foil. (iv) The temporal change (the ‘‘dose’’ change) of  $M/I$  for a sudden change of the current density has a similar dose constant ( $\sim 7 \text{mC}/\text{cm}^2$  in this example) to the initial transient.

A similar experiment was carried out with the neutral helium  $2^1P-3^1D$  line. In Fig. 4 are shown the results similar to those in Fig. 2. The beam energy is 150 keV. The open circles show  $M/I$  for  $28 \mu\text{A}/\text{cm}^2$ , and the open squares for  $8 \mu\text{A}/\text{cm}^2$ . The dose dependence was fitted by Eq. (1). The result of  $[M/I]_0$  and  $[M/I]_S$  is given in Fig. 5 along with those for other current densities. The filled circles in Fig. 4 represent the change of  $M/I$  when the beam current density is changed from  $26 \mu\text{A}/\text{cm}^2$  to  $8 \mu\text{A}/\text{cm}^2$  at  $9 \text{mC}/\text{cm}^2$ . A similar behavior to Fig. 2 is seen.

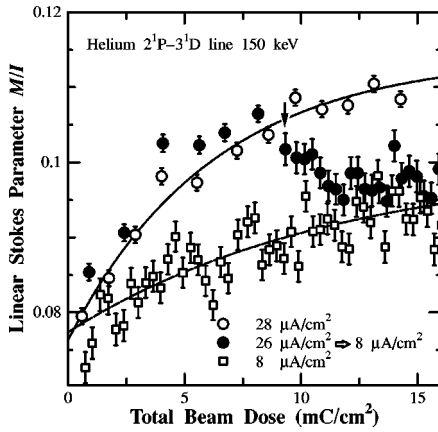


FIG. 4. The linear Stokes parameter  $M/I$  of the helium  $2^1P-3^1D$  line against the beam dose. The abscissa is similar to Fig. 2. The open circles are for  $28 \mu\text{A}/\text{cm}^2$ , and the open squares for  $8 \mu\text{A}/\text{cm}^2$ . The filled circles represent the  $M/I$  when the beam current density was started with  $26 \mu\text{A}/\text{cm}^2$  and at  $9 \text{mC}/\text{cm}^2$  it was changed to  $8 \mu\text{A}/\text{cm}^2$ . The vertical arrow represents the first datum with the lower density.

We may conclude that the four conclusions drawn for the Balmer  $\alpha$  line are also valid for the helium  $2^1P-3^1D$  line with an important exception. That is,  $[M/I]_0$  has much less dependence on the current density, or it is even independent of the density.

#### IV. DISCUSSION

In Figs. 2 and 4, the time scale of the change of  $M/I$  is the order of 10 min. All the models, except for the beam dose effect, mentioned in the Introduction, are inconsistent with this slow change: e.g., the characteristic time for the surface charge to reach a steady state is less than  $10^{-13}$  s, and the time for the foil temperature is less than 1 s. It would thus be natural to assume as its cause a change of the condition, or the state, of the foil with accumulation of the dose. This is in accordance with the conclusion of Ref. [16]. All the features in Sec. III are consistent with this explanation.

The initial value of the linear Stokes parameter  $[M/I]_0$  shown in Fig. 3 or Fig. 5 represents the  $M/I$  from the atoms excited by the virgin amorphous foil. In order to explain the current density dependence of  $[M/I]_0$ , we adopt the macroscopic field model [13,14] with the following simple assumptions: (i) A uniform charges distribution (surface density  $\varsigma$ ) develops on the foil and the charges produce the field  $F(z)$ , which is parallel to the beam direction ( $+z$ ),

$$F_z(z) = F_0 \left[ 1 - \frac{z}{\sqrt{a^2 + z^2}} \right], \quad (2)$$

where  $F_0 = \varsigma/2\epsilon_0$  is the field strength at the foil surface,  $\epsilon_0$  is the permittivity of vacuum,  $a$  is the foil radius, and  $z=0$  at the foil surface. (ii) The field strength  $F_0$  is proportional to the beam current density and is independent of the irradiated ion species to the foil.

The broken curve shown in Fig. 3 is the result of  $M/I$ . In the calculation we have adopted the initial population  $\sigma_{l,m_l}$  at the foil surface:  $\sigma_{s_0} = 0.500$ ,  $\sigma_{p_0} = 0.060$ ,  $\sigma_{p_1} = 0.120$ ,  $\sigma_{d_0}$

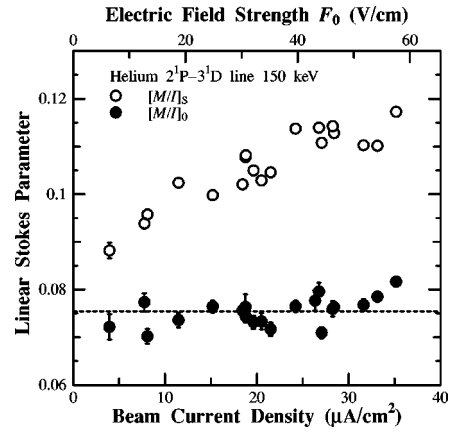


FIG. 5. The beam current density dependence of the initial value  $[M/I]_0$  (filled circles) and the saturated value  $[M/I]_S$  (open circles). The broken line represents the calculated  $M/I$  with the macroscopic field model.

$= 0.030$ ,  $\sigma_{d_1} = 0.040$ ,  $\sigma_{d_2} = 0.045$ , and all the coherence terms are assumed absent. The detail of the calculation procedure is given in Ref. [17]. The top abscissa represents the field strength  $F_0$  determined from the fitting. The field dependence is due to the Stark mixing of the H ( $n=3$ ) levels. The agreement is reasonable. The relatively large scatter (the reduced chi square is 4.8) of the experimental results may be attributed to individual characteristics (for example, the surface density) of each foil and our neglect of the coherence in the calculation, especially for the lower current density.

A similar calculation was carried out for the helium line with the same field strengths. The result is shown in Fig. 5 by the broken line. The populations are  $\sigma_{s_0} = 0.700$ ,  $\sigma_{p_0} = 0.118$ ,  $\sigma_{p_1} = 0.081$ ,  $\sigma_{d_0} = 0.005$ ,  $\sigma_{d_1} = 0.004$ ,  $\sigma_{d_2} = 0.003$ . The total populations of three levels ( $^1S$ ,  $^1P$ ,  $^1D$ ) are based on Ref. [8] and the alignment of  $^1P$  on Ref. [5], and the breakdown of the  $^1D$  population into the three (five) magnetic sublevels is determined from the fitting in Fig. 5. Virtually no field dependence is seen. It means that the He ( $n=3$ ) levels are not mixed by the field of this range. (Thus the polarization of the  $2^1P-3^1D$  line depends only on the latter three populations.) A field strength over  $10^4$  V/cm would be needed to produce Stark mixing and thus an obvious change in the polarization.

From the above discussions, it may be suggested that the current density dependence of  $[M/I]_S$  of helium is due solely to the beam dose effect, while that of hydrogen is a combination of this effect and the macroscopic field.

The beam foil spectroscopy has been and still is a powerful tool for the lifetime determination, and data on lifetime and oscillator strength of excited atoms and ions are being produced by this method. We hope the present findings contribute to improving the reliability of this method.

#### ACKNOWLEDGMENTS

The authors are especially grateful to Professor Takashi Fujimoto for many suggestions. We also wish to thank Sotaro Kawae, Tomohide Nakano, Dr. Rei Okasaka, Motoshi Goto, and Yoshiho Seo for their help.

- [1] H.G. Berry, L.J. Curtis, D.G. Ellis, and R.M. Schectman, Phys. Rev. Lett. **32**, 751 (1974).
- [2] T.G. Eck, Phys. Rev. Lett. **33**, 1055 (1974).
- [3] H.G. Berry, S.N. Bhardwaj, L.J. Curtis, and R.M. Schectman, Phys. Lett. **50A**, 59 (1974).
- [4] H.G. Berry, L.J. Curtis, and R.M. Schectman, Phys. Rev. Lett. **34**, 509 (1975).
- [5] R.L. Brooks, and E.H. Pinnington, Phys. Rev. A **18**, 1454 (1978).
- [6] M. Lombardi, Phys. Rev. Lett. **35**, 1172 (1975).
- [7] Y.B. Band, Phys. Rev. A **13**, 2061 (1976).
- [8] J.P. Weber, J.C. Dehaes, and J. Devooght, Phys. Rev. A **45**, 307 (1992).
- [9] R.D. Hight, R.M. Schectman, H.G. Berry, G. Gablielse, and T. Gay, Phys. Rev. A **16**, 1805 (1977).
- [10] H. Winter, Nucl. Instrum. Methods Phys. Res. **194**, 357 (1982).
- [11] T.J. Gay and H.G. Berry, Phys. Rev. A **19**, 952 (1979).
- [12] T.J. Gay, H.G. Berry, R. DeSerio, H.P. Garnir, R.M. Schectman, N. Schaffel, R.D. Hight, and D.J. Burns, Phys. Rev. A **23**, 1745 (1981).
- [13] W. Singer, J.C. Dehaes, and J. Carmeliet, Phys. Scr. **21**, 165 (1980).
- [14] J.C. Dehaes, J. Carmeliet, and H.G. Berry, Phys. Rev. A **40**, 5583 (1989).
- [15] J.W. Keller, K.W. Oglivie, J.W. Boring, and R.W. McKemie, Nucl. Instrum. Methods Phys. Res. B **61**, 291 (1991).
- [16] D.L. Harper, R.G. Albridge, N.H. Tolk, W. Qi, D.D. Allred, and L.V. Knight, Phys. Rev. A **52**, 4631 (1995).
- [17] Y. Kimura, T. Nishida, and K. Ishii, Phys. Rev. A **56**, 4612 (1997).